Chemical Science

Accepted Manuscript

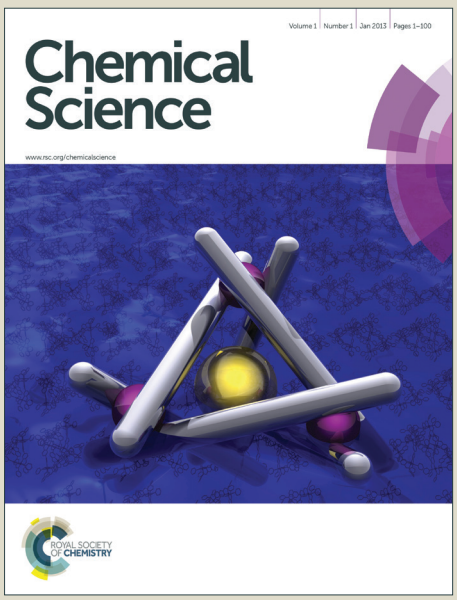

ROYAL SOCIETY OF CHEMISTRY

www.rsc.org/chemicalscience

Cite this: DOI: 10.1039/c0xx00000x

www.rsc.org/chemicalscience

EDGE ARTICLE

Doping-induced memory effect in Li-ion batteries: the case of Al-doped $Li_4Ti_5O_{12}$

De Li,[a] Yang Sun,[a] Xizheng Liu,[a] Ruwen Peng[c] and Haoshen Zhou*[a,b]

Received (in XXX, XXX) Xth XXXXXXXXX 20XX, Accepted Xth XXXXXXXXX 20XX

DOI: 10.1039/b000000x

In Li-ion batteries (LIBs), memory effect has been revealed in two-phase electrode materials as olivine $LiFePO_4$ and anatase TiO_2, which complicates two-phase transition and influences the estimation of the state of charge. Practical electrode materials are usually optimized by element doping strategy, while its impact on memory effect has not been reported yet. Here we firstly report the doping-induced memory effect in LIBs. Pristine $Li_4Ti_5O_{12}$ is free from memory effect, while distinct memory effect could be induced by Al-doping. After discharged to a lower cutoff potential, Al-doped $Li_4Ti_5O_{12}$ exhibits poorer electrochemical kinetics, delivering a larger overpotential during the charging process. This dependence of overpotential on the discharging cutoff leads to the memory effect in Al-doped $Li_4Ti_5O_{12}$. Our discovery emphasizes the impact of element doping on the memory effect of electrode materials, and thus has implications on the battery design.

Introduction

Li-ion batteries (LIBs) are the state-of-the-art power sources for mobile electrical devices, electric vehicles and smart grid.[1] It was generally accepted that LIBs are free from memory effect,[2] which is common in nickel-cadmium (Ni-Cd) and nickel-metal-hydride (Ni-MH) batteries.[3-5] However, recent studies indicated that the memory effect also exists in olivine $LiFePO_4$ and anatase TiO_2 in LIBs.[6, 7] As both $LiFePO_4$[8, 9] and TiO_2[10] undergo a two-phase reaction upon charge/discharge,[11-13] which leads to a very flat potential plateau, even minimal potential changes from memory effect will make it difficult to estimate the state of charge (SOC) in LIBs.

The memory effect of olivine $LiFePO_4$ cathode was firstly reported by Sasaki et al.,[6] which was rationalized by using the particle-by-particle model.[14] In the memory-writing cycle, $LiFePO_4$ particles are divided into two groups: part of $LiFePO_4$ particles (first group) undergoes an extra charge/discharge cycle relative to the others (second group). In the memory-releasing cycle, the second group is (dis)charged with a larger overpotential compared with the first group, which results in a potential bump in the (dis)charging curve. Memory effect is closely associated with the overshooting phenomena at the beginning of (dis)charging.[6, 7] Owing to a much smaller initial overshoot, no memory effect has been observed in spinel $Li_4Ti_5O_{12}$.[6]

Practical electrode materials are usually optimized by element doping strategy,[15] while its impact on the memory effect remains unknown. In this paper, we try to examine the impact of doping strategy, and we focus on spinel $Li_4Ti_5O_{12}$,[16] which is a renowned long-cycle-life anode material for LIBs.[17, 18] Although pristine $Li_4Ti_5O_{12}$ is free from memory effect, we find that a distinct memory effect could be induced by Al-doping.

Experimental

Pristine $Li_4Ti_5O_{12}$ (LTO) is provided by Ishihara Sangyo Kaisha, Ltd. and Nano-Al_2O_3 (mean particle size: 22.2~47.7 nm) is supplied by Nanophase Technologies Corp. (NanoTek®). LTO and nano-Al_2O_3 (10 wt.%) are ground thoroughly and the mixture is calcined at 800ºC for 24h in vacuum, to obtain Al-doped $Li_4Ti_5O_{12}$ (ALTO). The morphologies and crystal structures are characterized by scanning electron microscopy (SEM, LEO Gemini Supra 35) and powder X-ray diffraction (XRD, Cu Kα radiation, Bruker D8 Advance Diffractometer), respectively. The galvanostatic and voltammetric measurements are carried out at room temperature with a battery charge/discharge system from Hokuto Denko Corp. and an Autolab electrochemical instrument, respectively.

Electrochemical measurements are conducted by using coin cells (CR2032). In the working electrode, a composite paste, containing 42.5 wt.% LTO or ALTO, 42.5 wt.% acetylene black and 15 wt.% polytetrafluoroethylene (PTFE), is firmly pressed on an Al mesh (100 mesh) with a mass loading of *ca.* 4 mg cm^{-2}.

[a] *Energy Technology Research Institute, National Institute of Advanced Industrial Science and Technology (AIST), Umezono, 1-1-1, Tsukuba, 305-8568, Japan. Fax: +81-29-861-3489; E-mail: hs.zhou@aist.go.jp*

[b] *National Laboratory of Solid State Microstructures & Department of Energy Science and Engineering, Nanjing University, Nanjing 210093, China.*

[c] *National Laboratory of Solid State Microstructures & Department of Physics, Nanjing University, Nanjing 210093, China.*

† Electronic Supplementary Information (ESI) available: XRD, SEM and EIS mesurements, and other related information. See DOI: 10.1039/c0xx00000x

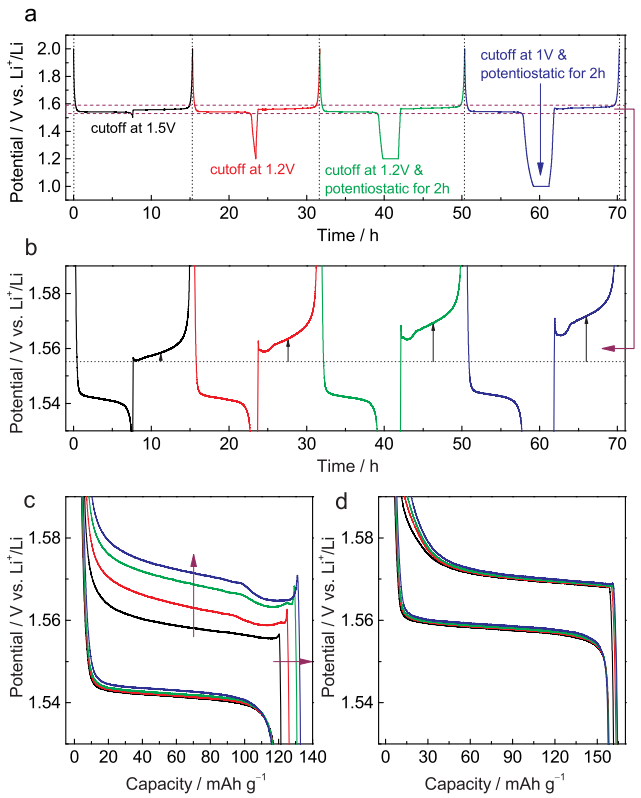

Fig. 1 Electrochemical dependence on the discharging cutoff in Al-doped $Li_4Ti_5O_{12}$ (ALTO). (a) A sequence of four cycles: (1) discharge to 1.5 V and full charge; (2) discharge to 1.2 V and full charge; (3) discharge to 1.2 V and potentiostatic for 2h, and full charge; (4) discharge to 1.0 V and potentiostatic for 2h, and full charge. (b) Enlarged view between 1.53 and 1.59 V. (c) The charge/discharge curves in these four cycles. (d) The charge/discharge curves in the same four cycles of pristine $Li_4Ti_5O_{12}$ (LTO). The current rate is 0.1C.

Here, 42.5 wt.% acetylene black is added to enhance the electronic conductivity. The counter electrode of lithium metal is separated from the working electrode by a Celgard 2400 porous polypropylene film, and the electrolyte is 1M $LiClO_4$ in ethylene carbonate/diethyl carbonate (EC/DEC with volume ratio of 1:1). After drying all components, the cells are assembled in a glovebox filled with argon gas.

Results and discussion

Fig. S1a shows X-ray diffraction (XRD) patterns of pristine $Li_4Ti_5O_{12}$ (LTO) and Al-doped $Li_4Ti_5O_{12}$ (ALTO). The XRD pattern of ALTO can be well indexed with the spinel structure, indicating no evident structural change after Al-doping, although minor amount of Al_2O_3 and rutile TiO_2 impurities exist. The peaks of ALTO shifts to higher angles compared with those of LTO (Fig. S1b), suggesting decreased lattice parameters, which is consistent with previous reports.[19, 20] Besides, both of the samples are assemblies of nano-crystallites (Fig. S2a-b).

Galvanostatic measurements were performed on ALTO in a sequence of four cycles with different discharging cutoffs (Fig. 1a). As the cutoff potential decreases, especially with potentiostatic, the subsequent charging potential heightens (Fig. 1b). Previous report has also indicated that the charging potential of Al-doped $Li_4Ti_5O_{12}$ heightens for the low discharging cutoff.[19]

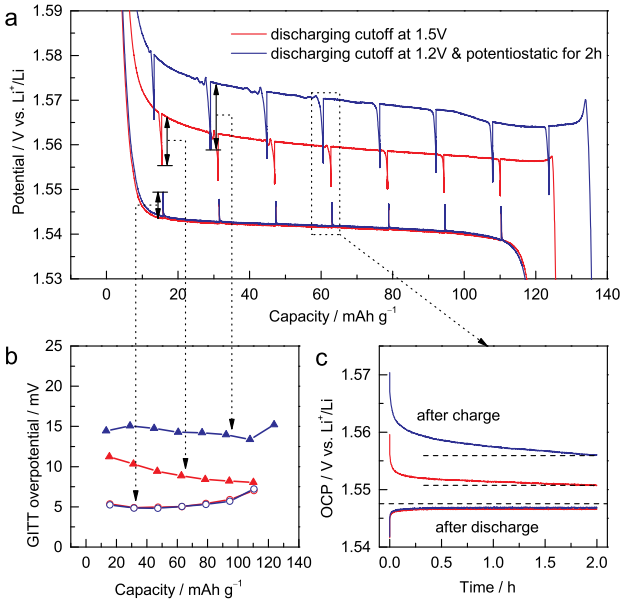

Fig. 2 (a) GITT measurements for Al-doped $Li_4Ti_5O_{12}$ (ALTO), which consist of a series of current pulses applied at 0.1C for 1h, each followed by a 2h relaxation period. The charging cutoff is 2.0 V, and the discharging cutoff is 1.5 V (red), 1.2V and potentiostatic for 2h (blue). (b) Potential increments (decrements) and (c) OCPs during the relaxation periods.

As the cutoff becomes lower, the capacity of subsequent charging is also increased (Fig. 1c). In the charging curves, a distinct overshoot appears at the beginning, the height of which is also dependent on the cutoff. For comparison, LTO was also measured following the same procedure, while the charging curves almost show no evident dependence on the discharging cutoff (Fig. 1d). Compared with LTO, the relatively low specific capacity of ALTO could be attributed to the impurities and Al-doping. Besides, the discharging potential of ALTO is lower than that of LTO, indicating that the Al-doping raises the energy of Ti^{4+}/Ti^{3+} redox couple in spinel $Li_4Ti_5O_{12}$.[21]

Also we examined the electrochemical dependence on the charging cutoff for ALTO (Fig. S3a). Results show that the discharging curves are independent of the charging cutoff (Fig. S3b). For different charging cutoffs, the subsequent discharging curves are nearly overlapped between these three cycles. Note that there is no overshoot at the beginning of discharging (Fig. S3c), consistent with the association between the memory effect and initial overshoot. For LTO, analogous results are obtained (Fig. S3d).

To study the electrochemical differences caused by different discharging cutoffs, galvanostatic intermittent titration technique (GITT) measurements [22] were performed on ALTO. For different cutoffs, the subsequent charging curves vary significantly (Fig. 2a). The potential decrement during relaxation in charging is also dependent on the cutoff: lower cutoff leads to larger potential decrement (Fig. 2b). Compared with the potential increments in discharging, the potential decrements in charging are much larger. During the relaxation in discharging, the open-circuit potential (OCP) almost approaches the equilibrium potential in two hours (Fig. 2c). In contrast, the OCP in charging continuously decreases as a tilted line, which is more evident for

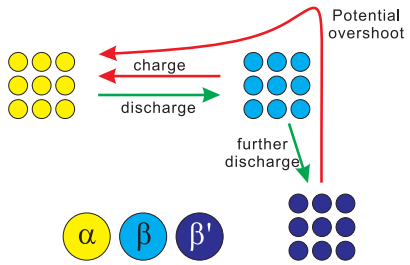

Fig. 3 Schematics of phase transition in Al-doped $Li_4Ti_5O_{12}$ under different discharging cutoffs, in which α is delithiated phase β is lithiated phase, and β′ is lithiated phase discharged to a very low cutoff potential.

the lower cutoff. These phenomena indicate that the kinetics of charging process, which is inferior to that of discharging process, is dependent on the discharging cutoff.

According to above results and analysis, we may infer that the status of ALTO electrode depends on the discharging cutoff, different from the undoped LTO. Fig. 1c-d shows that the specific capacity of ALTO increases with decreased discharging cutoff, while it almost remains constant in LTO. This indicates that a high discharging cutoff is enough to achieve the full lithiation of LTO. For ALTO, however, a few of Li sites is difficult to access and require a low discharging cutoff to realize the Li-ion insertion. These "hardly accessible" Li sites could be reasonably attributed to the Al-doping induced local structural change, while the detailed lattice structure after doping is still unknown and needs more investigations. Fig. 3 schematically illustrates the phase transition behaviour of ALTO with different discharging cutoffs. In the case of high cutoff, the phase transition between the α (delithiated) and β (lithiated) phases could occurs readily. Further discharging to a low cutoff, the β phase will be transformed into the β′ phase, which represents the lithiated phase after the deeper discharging, relative to the β phase. In the subsequent charging process, a high potential is necessary to convert the β′ phase into the α phase, owing to its poor electrochemical kinetics. The poor kinetics of β′ phase could also be reflected in the high initial overshoot during the charging process.

To identify the difference between β and β′ phases, the discharged ALTO with different discharging cutoffs was characterized using electrochemical impedance spectroscopy (EIS). The electrode was firstly discharged to different cutoff potentials and subsequently charged to 1.5V, then the corresponding EIS spectra were measured from 10^6 Hz to 10^{-3} Hz (Fig. S4). In the high frequency region, the depressed semicircle (the inset in Fig. S4b) is associated with the charge-transfer resistance (Rct), which barely changes for different discharging cutoffs. In the low frequency, the bounded-diffusion impedance exhibits a transition from the Warburg regime to the capacitive regime by decreasing the frequency (Fig. S4b),[23] and it enlarges evidently for the lower discharging cutoff (Fig. S4b-c). In other words, the diffusion impedance of β′ phase is larger than that of β phase for discharged ALTO, validating the difference in electrochemical kinetics. In contrast, no evident difference was found in the EIS spectra of LTO with different discharging cutoffs (Fig. S5).

The dependence of charging potential on the preceding discharging cutoff is equivalent to a memory effect in LIBs.

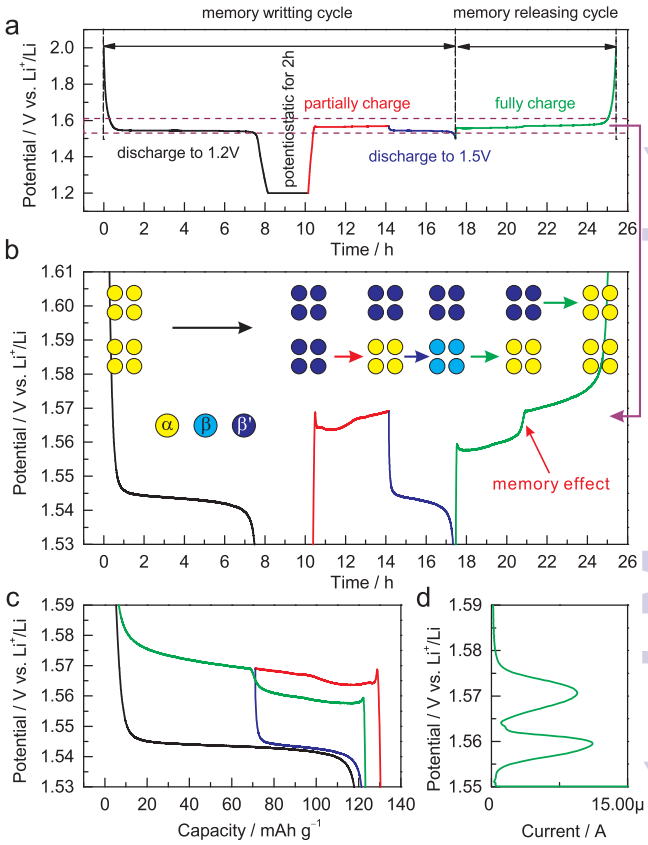

Fig. 4 Demonstration of a memory effect in Al-doped $Li_4Ti_5O_{12}$ (ALTO). (a) Memory-writing cycle: discharge to 1.2 V and potentiostatic for 2h (black), partially charge for 4h (red), and discharge to 1.5 V (blue); memory-releasing cycle: full charge to 2.0 V (green). The current rate is 0.1C. (b) Enlarged view between 1.53 and 1.61 V. The inset shows corresponding phase transition, in which α is delithiated phase, β is lithiated phase discharged to 1.5 V, and β′ is lithiated phase discharged to 1.2 V and potentiostatic for 2h. (c) The charge/discharge curves in these memory-writing/releasing cycles. (d) The Linear Sweep Voltammetry (LSV) curve of ALTO with a scan rate of 1μV s^{-1} from 1.55 to 1.59 V after the same memory-writing cycle.

Analogous to the reported memory effect in olivine $LiFePO_4$ and anatase TiO_2,[6, 7] ALTO exhibits a two-step charging curve after a special memory-writing cycle, which is a typical memory effect (Fig. 4a-b). The corresponding phase transition can be described by a schematic model (Fig. 4b). Firstly, all particles in the electrode are discharged to 1.2 V and potentiostatic for 2h; secondly, a group of particles (lower) are charged and then discharged to 1.5 V, while the other group (upper) has not changed; then, the lower group with the discharging cutoff of 1.5 V is charged first at a low potential, followed by the charging of the upper group at a high potential. Although the charging process from the low discharging cutoff is interrupted by a partial discharge/charge cycle (blue curve and the lower step of green curve), the charging curve can still be smoothly connected as the red curve and the higher step of green curve (Fig. 4c). The memory effect can also be reflected by Linear Sweep Voltammetry (LSV) result (Fig. 4d). The two peaks in the LSV mode correspond to the two steps in the galvanostatic mode. These results unambiguously demonstrate the memory effect in the electrochemical processes of ALTO. By comparison, no memory effect has been observed in LTO (Fig. S6).

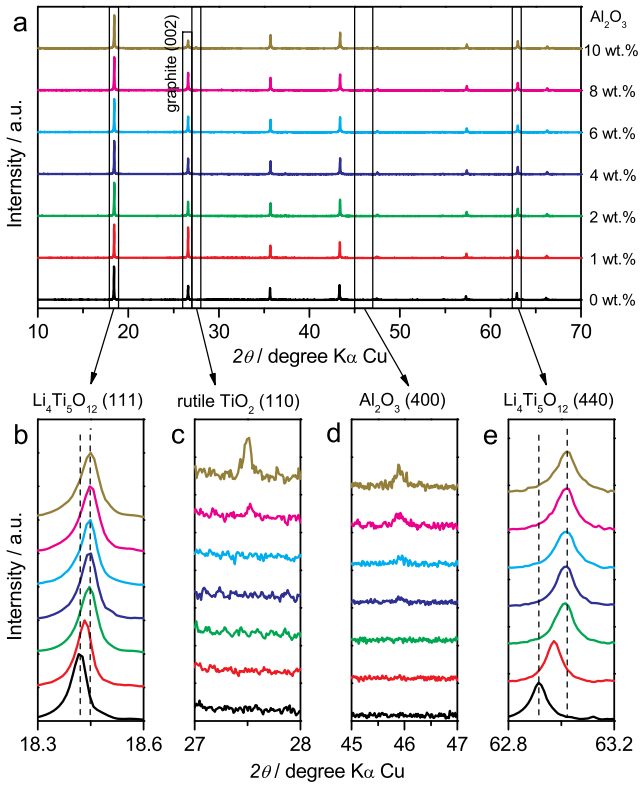

Fig. 5 (a) XRD patterns of Al-doped $Li_4Ti_5O_{12}$ with different doping levels. In the precursor, the amount of Al_2O_3 is varied from 0 wt.% to 10 wt.%. Enlarged XRD patterns of (b) $Li_4Ti_5O_{12}$ (111), (c) rutile TiO_2 (110), (d) Al_2O_3 (400), (e) $Li_4Ti_5O_{12}$ (440) peaks. During XRD measurements, ca. 5 % graphite is mixed into the samples to calibrate the position of peaks.

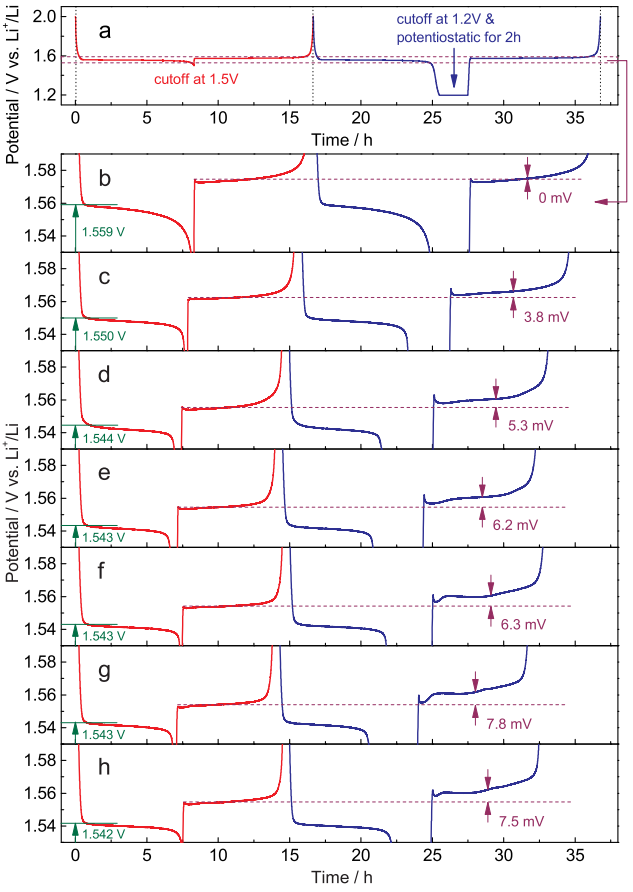

Fig. 6 Electrochemical dependence of Al-doped $Li_4Ti_5O_{12}$ on the doping level. (a) The sequence of two cycles. 1st cycle: discharge to 1.5 V and full charge; 2nd cycle: discharge to 1.2 V and potentiostatic for 2h, and full charge. Enlarged view between 1.53 and 1.59 V for Al-doped $Li_4Ti_5O_{12}$, the precursor of which contains (b) 0 wt.%, (c) 1 wt.%, (d) 2 wt.%, (e) 4 wt.%, (f) 6 wt.%, (g) 8 wt.%, and (h) 10 wt.% Al_2O_3. The charge/discharge current rate is 0.1C.

Besides LTO and ALTO above, we also studied a series of Al-doped $Li_4Ti_5O_{12}$ with different doping levels. The amount of nano-Al_2O_3 was varied from 0 wt.% to 10 wt.% in the precursor to change the doping level in Al-doped $Li_4Ti_5O_{12}$. The precursor of pristine $Li_4Ti_5O_{12}$ (Sigma-Aldrich Co. LLC.) and nano-Al_2O_3 mixture was ground thoroughly and calcined at 800ºC for 24h in air to obtain Al-doped $Li_4Ti_5O_{12}$. Fig. 5a shows XRD patterns of Al-doped $Li_4Ti_5O_{12}$ with different doping levels. The XRD peaks of Al-doped $Li_4Ti_5O_{12}$ shift towards higher angles as the amount of Al_2O_3 increases from 0 wt.% to 2 wt.%. Above 2 wt.%, the peaks of identical index approach a constant angle (Fig. 5b, 5e). Rutile TiO_2 appears when Al_2O_3 amount is over 8 wt.% (Fig. 5c), and Al_2O_3 residue increases as the amount of Al_2O_3 precursor is varied from 0 wt.% to 10 wt.% (Fig. 5d). Above results indicate that high-level Al-doping will lead to phase separation associated with the formation of rutile TiO_2.[24]

In galvanostatic measurements, a sequence of two cycles with different discharging cutoffs is performed on all these samples (Fig. 6). Results show that the initial potential of the discharge plateau significantly decreases before the doping content approaches saturation (Fig. S7a-b), further confirming that the energy of Ti^{4+}/Ti^{3+} redox couple in spinel $Li_4Ti_5O_{12}$ could be changed by Al-doping. Also we may see the charging potential increment arising from different discharging cutoffs (Fig. 6b-h) shows the same dependence on the doping content (Fig. S7c), suggesting that the memory effect of Al-doped $Li_4Ti_5O_{12}$ can be tailored by changing the doping level. Although a small amount of impurities, e.g., rutile TiO_2, could be introduced by high level doping, their effect on the memory effect is insignificant.

Conclusions

In this study, we show the Al-doping-induced memory effect in spinel $Li_4Ti_5O_{12}$ anode for LIBs. For Al-doped $Li_4Ti_5O_{12}$, the electrochemical kinetics, which shows up as overpotential, can be altered by changing the discharging cutoff. In a special memory-writing cycle, multiple discharging cutoffs can be recorded in a discharged electrode. In the following charge process, this information can be read as a stepped charging curve, which is memory effect. The memory effect of Al-doped $Li_4Ti_5O_{12}$ could be rationalized on the basis of the particle-by-particle model. Besides, memory effect can be tailored by changing the doping level in Al-doped $Li_4Ti_5O_{12}$. Our discovery demonstrates that the widely adopted element doping strategy is noteworthy in triggering memory effect in LIBs, which should be taken into account in industrial battery design.

Notes and references

1. M. Armand and J. M. Tarascon, *Nature*, 2008, **451**, 652-657.

2. Y. Nishi, *J Power Sources*, 2001, **100**, 101-106.
3. G. Davolio and E. Soragni, *J Appl Electrochem*, 1998, **28**, 1313-1319.
4. R. A. Huggins, *Solid State Ionics*, 2006, **177**, 2643-2646.
5. Y. Sato, S. Takeuchi and K. Kobayakawa, *J Power Sources*, 2001, **93**, 20-24.
6. T. Sasaki, Y. Ukyo and P. Novak, *Nat Mater*, 2013, **12**, 569-575.
7. E. Madej, F. L. Mantia, W. Schuhmann and E. Ventosa, *Adv Energy Mater*, 2014, 1400829.
8. Y. G. Wang, P. He and H. S. Zhou, *Energy & Environmental Science* 2011, **4**, 805-817.
9. L. X. Yuan, Z. H. Wang, W. X. Zhang, X. L. Hu, J. T. Chen, Y. H. Huang and J. B. Goodenough, *Energy & Environmental Science*, 2011, **4**, 269-284.
10. C. H. Jiang and J. S. Zhang, *J Mater Sci Technol*, 2013, **29**, 97-122.
11. A. Yamada, H. Koizumi, S. I. Nishimura, N. Sonoyama, R. Kanno, M. Yonemura, T. Nakamura and Y. Kobayashi, *Nat Mater*, 2006, **5**, 357-360.
12. R. Malik, A. Abdellahi and G. Ceder, *J Electrochem Soc*, 2013, **160**, A3179-A3197.
13. M. Wagemaker, W. J. H. Borghols and F. M. Mulder, *J Am Chem Soc*, 2007, **129**, 4323-4327.
14. W. Dreyer, J. Jamnik, C. Guhlke, R. Huth, J. Moskon and M. Gaberscek, *Nat Mater*, 2010, **9**, 448-453.
15. S. Y. Chung, J. T. Bloking and Y. M. Chiang, *Nat Mater*, 2002, **1**, 123-128.
16. G. N. Zhu, Y. G. Wang and Y. Y. Xia, *Energy & Environmental Science*, 2012, **5**, 6652-6667.
17. T. Ohzuku, A. Ueda and N. Yamamoto, *J Electrochem Soc*, 1995, **142**, 1431-1435.
18. K. Ariyoshi, R. Yamato and T. Ohzuku, *Electrochim Acta*, 2005, **51**, 1125-1129.
19. Z. H. Wang, G. Chen, J. Xu, Z. S. Lv and W. Q. Yang, *J Phys Chem Solids*, 2011, **72**, 773-778.
20. H. L. Zhao, Y. Li, Z. M. Zhu, J. Lin, Z. H. Tian and R. L. Wang, *Electrochim Acta*, 2008, **53**, 7079-7083.
21. J. B. Goodenough and Y. Kim, *Chem Mater*, 2010, **22**, 587-603.
22. W. Weppner and R. A. Huggins, *J Electrochem Soc*, 1977, **124**, 1569-1578.
23. J. H. Song and M. Z. Bazant, *J Electrochem Soc*, 2013, **160**, A15-A24.
24. G. N. Zhu, L. Chen, Y. G. Wang, C. X. Wang, R. C. Che and Y. Y. Xia, *Adv Funct Mater*, 2013, **23**, 640-647.